Modeling Time-Varying Aggregate Interference from Cognitive Radios and Implications on Primary Exclusive Zone Design

Mohd. Shabbir Ali, Neelesh B. Mehta, *Senior Member, IEEE*

Abstract—Accurately characterizing the time-varying nature of the aggregate interference from secondary users (SUs) is essential in ensuring a successful deployment of a cognitive radio (CR) network. This requires characterizing the probability distribution and the time-varying nature of the aggregate interference from multiple SUs. We show that it is well modeled as a shifted lognormal random process, and is more accurate than the lognormal, Gaussian, and symmetric truncated stable models considered in the literature even for a relatively dense deployment of SUs. Our model accounts for the effect of imperfect spectrum sensing, which depends on path loss, shadowing, and fading of the link from primary transmitter to the SU, and the randomness in the number of SUs and their locations. It also allows for both interweave and underlay modes of CR operation. We also demonstrate the relevance of the proposed analytically tractable model in the design of the primary exclusive zone.

I. INTRODUCTION

A common paradigm of cognitive radio (CR) classifies users as primary users (PUs), which have unfettered access to the spectrum, and secondary users (SUs), which can use the spectrum but under tight constraints on the interference their transmissions cause to the PUs [1]–[4]. A successful design and deployment of CR, therefore, requires an accurate model for the aggregate interference. This characterization feeds into the design of transmission policies for SUs and techniques to help mitigate their interference.

A multitude of factors must be considered together in order to arrive at an accurate statistical model for the aggregate interference. It is affected by propagation characteristics of the channels between the SUs and PUs, such as path loss, shadowing, and fading. Furthermore, the number of SUs that transmit and their locations themselves are random variables (RVs) and affect the interference. Imperfect spectrum sensing also directly affects the interference process as it determines the SUs' transmit powers and whether or not they transmit.

Given the importance of interference modeling in CR, one of the approaches pursued for it is based on measurements. In [5], co-channel and adjacent channel interference at a television receiver from an SU transmitter (SU-Tx) are measured. In [6], interference measurements for fixed indoor and outdoor geometries are presented. In [7], interference cartography,

The authors are with the Dept. of Electrical Communication Eng. at the Indian Institute of Science (IISc), Bangalore, India.

Emails: mdshabbirali88@gmail.com, nbmehta@ece.iisc.ernet.in

which is a map of the interference measured over a region, is presented. However, the above models, while accurate, are very location-specific. Therefore, a second approach has focused on developing statistical models [1]–[4]. However, no closed form exists for the probability distribution function (PDF) of the aggregate interference. Therefore, the following approximate analytical models have been investigated.

Interference in Underlay Mode: In the underlay mode, an SU can transmit even when it senses that the PU is transmitting. However, it does so with a much lower power in order to avoid excessive interference to the PU receiver (PU-Rx). In [1], the aggregate interference at the PU-Rx from a fixed number of SUs, which are distributed uniformly over a region, is modeled as a lognormal RV. However, only large-scale shadow fading is taken into account. A spatial Poisson point process (SPPP) model is instead assumed for the SU locations in [2], and the aggregate interference is again modeled as a lognormal RV. However, in [1] and [2], the effect of imperfect spectrum sensing by the SUs is not accounted for.

Interference in Interweave Mode: In the interweave mode, an SU transmits only when it senses the PU to be off [8]. In [3], the aggregate interference is modeled as a symmetric truncated-stable (STS) RV. Compared to the Stable distribution model that had been used earlier in [9] to model the aggregate interference, the STS model ensures that its second and higher moments are finite. The SUs are distributed as per the SPPP model and use an energy detector (ED) for spectrum sensing. In [4], the aggregate interference is modeled as a shifted lognormal (SLN) RV, again assuming an SPPP model for the SUs. Spectrum sensing with and without cooperation using an ED is considered.

A. Contributions and Comparisons with Existing Literature

We develop a model that captures the snapshot statistics, i.e., PDF, as well as the time-varying statistics of the aggregate interference. We show that the aggregate interference is well modeled as an SLN random process (RP) except when it is very small. Modeling the time-varying nature is important because it affects the PU. For example, in [10], it has been argued that long dips in the signal-to-noise-plus-interference-ratio are detrimental to the PUs. Our model accounts for imperfect spectrum sensing, which depends on the location of the SU relative to the PU-Tx. Our model allows the SUs

to operate in both the interweave and underlay modes. In the interweave mode, interference occurs due to imperfect spectrum sensing by the SUs, and in the underlay mode, it occurs due to concurrent transmissions by the SUs when the PU-Tx is transmitting. Also, it accounts for the combined effect of time-correlated shadowing and small-scale Rayleigh fading in the various links. The randomness in the SU locations and numbers is also captured using the homogeneous SPPP model. We also extensively benchmark the proposed model with other statistical models proposed in the literature.

Another contribution of the paper is the application of the proposed model for improving the design of the primary exclusive zone (PEZ) [11], [12]. The PEZ is defined as the region around the PU-Rx within which no SU is allowed to transmit. Our redesign of the PEZ constrains not only the probability that the aggregate interference exceeds a threshold but also its average exceedance duration (AED). Thus, the time-varying nature of the interference is also accounted for.

Comparisons and Comments: While the SLN model has been considered before in the literature, its use and the verification of its ability to model the aggregate interference from the SUs when all the above physical layer effects are accounted for is new and challenging, and is a contribution of this paper. Our approach generalizes in several ways the SLN model considered in [4]. It is also more general than the level crossing rate (LCR) analysis in [13], which considers a system with one SU and one PU, only models shadowing, and assumes perfect spectrum sensing. While the aggregate interference is instead modeled as a gamma RP in [14], shadowing and imperfect spectrum sensing are not modeled and the number of interferers is fixed.

While the Stable model [9] is provably exact in the asymptotic regime of a large number of SUs, generalizing it or the STS model to incorporate the time-varying nature of interference is an open problem. These two models also require accurate, numerically stable techniques to compute the PDF from the characteristic function that they analytically characterize. Furthermore, we show that the STS model is less accurate than the proposed SLN model, despite the latter's simplicity and tractability, except at very high SU densities.

Our PEZ design approach also differs from that in [11], which did not consider imperfect spectrum sensing, shadowing, small-scale fading, and time-variations. Similarly, in the PEZ design in [12], imperfect spectrum sensing and time variations are not considered.

The paper is organized as follows. Section II describes the system model. The aggregate interference process model is developed in Section III. Simulation results and PEZ redesign are presented in Section IV. Conclusions follow in Section V.

II. SYSTEM MODEL

We shall use the following notation. Expectation is denoted by $\mathbb{E}[.]$ and the notation $X(t) \sim \mathcal{N}(\mu_X, \sigma_X^2, C_X(\tau))$ shall mean that $X(t)$ is a wide sense stationary (WSS) Gaussian
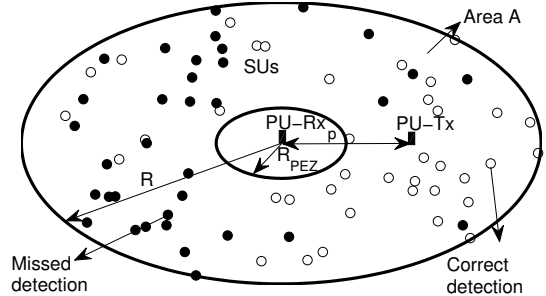
Fig. 1. System model showing the SUs that are scattered over a region using a homogeneous SPPP. Each SU performs spectrum sensing using an ED.

RP with mean μ_X, variance σ_X^2, and covariance function $C_X(\tau)$. Similarly, $X \sim \mathcal{N}(\mu_X, \sigma_X^2)$ denotes a Gaussian RV. An exponential RV X with mean μ is denoted by $X \sim \exp(\mu)$.

System Layout: Figure 1 shows the system layout considered. The number and locations of the SUs is modeled as a homogeneous SPPP, which is characterized by a density parameter Υ. The number of SUs N_{CR} that occur in a region of area $A = \pi \left(R^2 - R_{PEZ}^2 \right)$ is a Poisson distributed RV with mean ΥA. Here, R_{PEZ} is the radius of the PEZ around the PU-Rx, within which no SU is allowed to transmit [11], [12]. The PU-Rx is located at the center of the region and the PU-Tx is located at a distance p from the PU-Rx.

Channel Model: The large-scale shadowing is modeled as a lognormal RP and the small-scale fading is modeled as a Rayleigh RP [15]. Therefore, the power received at the PU-Rx located at a distance $r_i(t)$ from the ith SU is given by

$$PK \left(\frac{d_0}{r_i(t)} \right)^{\eta} e^{\beta X_i(t)} h_i(t), \tag{1}$$

where P is the transmit power of the SU. The path loss component is $K \left(\frac{d_0}{r_i(t)} \right)^{\eta}$, where $K = \left(\frac{\lambda}{4\pi d_0} \right)^2$, λ is the carrier wavelength, d_0 is the break point distance, and η is the path loss exponent [16, Chap. 2].

The shadowing component is $e^{\beta X_i(t)}$, where $\beta = \log 10/10$ and $X_i(t) \sim \mathcal{N}\left(0, \sigma_{x_i}^2, C_{x_i}(\tau)\right)$. The covariance function $C_{x_i}(\tau)$ is given by the modified Gudmundson's model as [10]

$$C_{x_i}(\tau) = \sigma_{x_i}^2 \exp \left(-\frac{v^2 \tau^2}{2D^2} \right), \tag{2}$$

where v is the speed of the SU and D is the decorrelation distance. The Rayleigh fading component is $h_i(t) \sim \exp(1)$. Its normalized covariance function $C_{h_i}(\tau)$ is given as per the Jakes' fading model as [15]

$$C_{h_i}(\tau) = J_0^2 \left(2\pi f_m \tau \right), \tag{3}$$

where f_m is the maximum Doppler spread and J_0 is the Bessel function of the first kind of order zero [17]. The shadowing and fading seen by different SUs on their links from the PU-Tx and to the PU-Rx are independent and identically distributed.

Spectrum Sensing (SS): The accuracy of SS by the SU depends on the channel gain of the link from the PU-Tx to the SU. We illustrate the dependence using the ED of [18]. If the energy received by the SU from the PU-Tx over a time T and bandwidth B exceeds a threshold ξ then the PU-Tx is detected to be on.

The probability P_{FA} of detecting the PU-Tx to be on given that it is off is $P_{\text{FA}} = Q\left(\frac{\xi - N_0 TB}{N_0^2 TB}\right)$, where N_0 is the noise power and Q is the standard Gaussian Q function. The probability $P_D(q_i, Y_i, g_i)$ of correctly detecting the PU-Tx to be on given that it is on, depends on the signal-to-noise-ratio (SNR) $\gamma(q_i, Y_i, g_i)$ at the ith SU, which is a function of the distance q_i of the SU from the PU-Tx, shadowing $e^{\beta Y_i}$, and Rayleigh fading g_i during the time duration of sensing. Here, $Y_i \sim \mathcal{N}\left(0, \sigma_{y_i}^2\right)$ and $g_i \sim \exp(1)$. The expression for $P_D(q_i, Y_i, g_i)$ in terms of P_{FA} is

$$P_D(q_i, Y_i, g_i) = Q\left(\frac{Q^{-1}(P_{\text{FA}}) - \gamma(q_i, Y_i, g_i)\sqrt{TB}}{\sqrt{1 + 2\gamma(q_i, Y_i, g_i)}}\right). \quad (4)$$

Note that other models for SS can be used [19]; this only changes the expressions of P_{FA} and P_D.

SU Transmission and Interference Model: If the SU detects the PU-Tx to be on, which we refer to as hypothesis H_1, then it operates in the underlay mode and transmits with a lower power P_u. Else, if the SU detects the PU-Tx to be off, which we refer to as hypothesis H_0, then it operates in the interweave mode and transmits with a higher power P_o. From (1), the interference power $I_i(t)$ at the PU-Rx from the ith SU, which is $r_i(t)$ distance away, is

$$I_i(t) = \begin{cases} P_u K\left(\frac{d_0}{r_i(t)}\right)^\eta e^{\beta X_i(t)} h_i(t), & \text{if } H_1 \text{ is detected,} \\ P_o K\left(\frac{d_0}{r_i(t)}\right)^\eta e^{\beta X_i(t)} h_i(t), & \text{if } H_0 \text{ is detected.} \end{cases} \quad (5)$$

III. INTERFERENCE MODELING

The aggregate interference at the PU-Rx from the SUs is

$$I_\Sigma(t) = \sum_{i=1}^{N_{CR}} I_i(t). \quad (6)$$

Our goal is to accurately model $I_\Sigma(t)$ when the PU-Tx is on. We model $I_\Sigma(t)$ as a WSS SLN RP, $I_\Sigma(t) \approx e^{Z(t)} + s$, where $Z(t) \sim \mathcal{N}\left(\mu_Z, \sigma_Z^2, C_Z(\tau)\right)$ and s is called the shift parameter. The parameters of $Z(t)$ are obtained in terms of the parameters of $I_\Sigma(t)$ by the moment-matching method [15]:

$$\sigma_Z^2 = \log\left(\frac{1}{4}\Gamma^{\frac{2}{3}} + 4\Gamma^{-\frac{2}{3}} - 1\right), \quad (7)$$

$$\mu_Z = \frac{1}{2}\left(\log\left(\frac{\kappa_2}{e^{\sigma_Z^2} - 1}\right) - \sigma_Z^2\right), \quad (8)$$

$$s = \kappa_1 - \exp\left(\mu_Z + \frac{1}{2}\sigma_Z^2\right), \quad (9)$$

$$C_Z(\tau) = \log\left(\Upsilon A \mathbb{E}[I_i(t) I_i(t+\tau)] + e^{2\mu_Z + \sigma_Z^2}\right) - \left(2\mu_Z + \sigma_Z^2\right), \quad (10)$$

where $\Gamma = 4\kappa_3 + 4\sqrt{4 + \kappa_3^2}$ and κ_m is the mth cumulant of $I_\Sigma(t)$, which can be shown to be $\kappa_m = \Upsilon A \mathbb{E}[I_i(t)^m]$. The expressions in (7), (8), and (9) are derived in [20], and (10) is derived in Appendix A.

Evaluation of the parameters of $Z(t)$ requires expressions for $\mathbb{E}[I_i(t)^m]$, for $m = 1, 2, 3$, and $\mathbb{E}[I_i(t) I_i(t+\tau)]$. As shown in Appendix B, $\mathbb{E}[I_i(t)^m]$, for $m \geq 1$, is given by

$$\mathbb{E}[I_i(t)^m] \approx \frac{2m! P_o^m K^m d_0^{m\eta}\left(R_{\text{PEZ}}^{2-m\eta} - R^{2-m\eta}\right)}{(m\eta - 2)\left(R^2 - R_{\text{PEZ}}^2\right)} e^{\frac{1}{2}m^2\beta^2\sigma_{x_i}^2}$$
$$- \frac{2m!\left(P_o^m - P_u^m\right)K^m}{\sqrt{\pi}W_c\left(R^2 - R_{\text{PEZ}}^2\right)} e^{\frac{1}{2}m^2\beta^2\sigma_{x_i}^2} \sum_{n_1=1}^{W_h} w_h(n_1) \sum_{n_2=1}^{W_l} w_l(n_2)$$
$$\times \sum_{n_3=1}^{W_c} \int_{R_{\text{PEZ}}}^R \frac{d_0^{m\eta}}{r_i^{m\eta-1}} P_D\left(q_i'(r_i, n_3), \sqrt{2}\sigma_{y_i} a_h(n_1), a_l(n_2)\right) dr_i. \quad (11)$$

Here $q_i'(r_i, n_3) = \sqrt{r_i^2 + p^2 - 2r_i p a_c(n_3)}$, $w_h(n)$ and $a_h(n)$, for $n = 1, \ldots, W_h$, denote the weights and the abscissas, respectively, of Gauss-Hermite quadrature; $a_c(n)$, for $n = 1, \ldots, W_c$, denote the abscissas of Gauss-Chebyshev quadrature; and $w_l(n)$ and $a_l(n)$, for $n = 1, \ldots, W_l$, denote the weights and the abscissas, respectively, of Gauss-Laguerre quadrature [17]. A key point to note is that the expressions are accurate even with a few terms; for the range of parameters that we consider, $W_c = W_h = W_l = 6$ suffice.

As shown in Appendix C, $\mathbb{E}[I_i(t) I_i(t+\tau)]$ is given by[1]

$$\mathbb{E}[I_i(t) I_i(t+\tau)] \approx \frac{P_o^2 K^2 d_0^{2\eta}\left(R_{\text{PEZ}}^{2-2\eta} - R^{2-2\eta}\right)}{(\eta - 1)\left(R^2 - R_{\text{PEZ}}^2\right)}$$
$$\times e^{\beta^2\sigma_{x_i}^2\left(1+\exp\left(-\frac{v^2\tau^2}{2D^2}\right)\right)} \left(J_0^2(2\pi f_m\tau) + 1\right)$$
$$- \frac{2\left(P_o^2 - P_u^2\right)K^2}{\sqrt{\pi}W_c\left(R^2 - R_{\text{PEZ}}^2\right)} e^{\beta^2\sigma_{x_i}^2\left(1+\exp\left(-\frac{v^2\tau^2}{2D^2}\right)\right)}$$
$$\times \left(J_0^2(2\pi f_m\tau) + 1\right) \sum_{n_1=1}^{W_h} w_h(n_1) \sum_{n_2=1}^{W_l} w_l(n_2)$$
$$\times \sum_{n_3=1}^{W_c} \int_{R_{\text{PEZ}}}^R \frac{d_0^{2\eta}}{r_i^{2\eta-1}} P_D\left(q_i'(r_i, n_3), \sqrt{2}\sigma_{y_i} a_h(n_1), a_l(n_2)\right) dr_i. \quad (12)$$

The expressions above in (11) and (12) cannot be simplified further because of the presence of the P_D term inside the integrand. They are mathematically involved because they take into account all the sources of randomness. However, as we saw, they are in the form of the single integrals that are easily evaluated numerically.

LCR and AED to Measure Time-varying Nature of Interference: For the SLN RP $I_\Sigma(t)$, the LCR $L_{I_\Sigma(t)}(I_{\text{th}})$ and AED

---

[1]The analysis assumes that any abrupt changes in $I_\Sigma(t)$ caused by a change in the decision of an SU about the PU-Tx being on or off is negligible.

for a threshold I_{th} can be obtained along lines similar to [14], [21], and can be shown to be

$$L_{I_{\Sigma(t)}}(I_{\text{th}}) = \frac{\sqrt{\Omega_Z}}{2\pi\sigma_Z} e^{-\frac{(\log(I_{\text{th}}-s)-\mu_Z)^2}{2\sigma_Z^2}}, \quad I_{\text{th}} > s, \quad (13)$$

$$\text{AED}_{I_{\Sigma(t)}}(I_{\text{th}}) = \frac{Q\left(\frac{\log(I_{\text{th}}-s)-\mu_Z}{\sigma_Z}\right)}{L_{I_{\Sigma(t)}}(I_{\text{th}})}, \quad I_{\text{th}} > s, \quad (14)$$

where $\Omega_Z = -\frac{d^2}{d\tau^2}C_Z(\tau)\big|_{\tau=0}$ is computed from (10) and (12).

IV. NUMERICAL RESULTS

We now evaluate the accuracy of the proposed model using Monte Carlo simulations, which use 10^5 drops. In each drop a random number of SUs and their locations are generated as per the SPPP. Each SU moves with a fixed velocity v in a random direction. Each SU performs SS as per Sec. II. The aggregate interference from all the SUs at the PU-Rx is then measured.

We use the following parameters in the simulations: PU-Tx transmit power: $P_{\text{Tx}} = 10$ dBm, SU transmit power in interweave mode: $P_o = 2$ dBm, SU transmit power in underlay mode: $P_u = -6$ dBm, noise power: $N_0 = -100$ dBm, density of SUs: $\Upsilon = 100$ SUs/km^2, system bandwidth: $B = 1$ MHz, carrier frequency: $f_c = 900$ MHz, radius of region considered: $R = 1000$ m, PEZ radius: $R_{\text{PEZ}} = 200$ m, distance between PU-Tx and PU-Rx: $p = 500$ m, path loss exponent: $\eta = 4$, standard deviation of shadow fading: $\sigma_{x_i} = \sigma_{y_i} = 6$, break-point distance: $d_0 = 10$ m, speed of SUs: $v = 5$ m/s, false alarm probability: $P_{\text{FA}} = 10\%$, and SS duration: $T = 50$ μs.

Snapshot Statistics: Figure 2 compares the cumulative distribution function (CDF) and the complementary CDF (CCDF) of $I_{\Sigma}(t)$ using the proposed model. The CDF evaluates the accuracy in matching smaller $I_{\Sigma}(t)$ values, while the CCDF evaluates the accuracy in matching larger $I_{\Sigma}(t)$ values, where the CDF saturates. Also shown are the corresponding results using the Gaussian, lognormal, and STS [3] models. In the lognormal model, $\log(I_{\Sigma}(t))$ is modeled as a Gaussian RP [21]. In the Gaussian model, which is motivated by the central limit theorem, $I_{\Sigma}(t)$ is modeled as a Gaussian RP. We see that the Gaussian and lognormal RP models are the least accurate. The STS model matches the CCDF better, but its CDF is inaccurate as it saturates for small values. For the given parameters, the SLN RP model matches the CCDF well and is more accurate than the other models for $I_{\text{th}} > -90$ dBm. This is because it matches the skewness of $I_{\Sigma}(t)$ better than the other models [4].

Time-varying Behavior: To evaluate the accuracy in modeling the time-variations of the aggregate interference, we study the LCR and AED of the various models. The LCR is shown in Fig. 3. The maximum value of the LCR depends on the velocity of the SUs, which can be inferred from the expression in (13). The Gaussian RP model is again very inaccurate. For $I_{\text{th}} < -90$ dBm, the lognormal RP model overestimates the LCR while the SLN RP model underestimates it, which is in line with Fig. 2. For $I_{\text{th}} > -90$ dBm, the proposed model
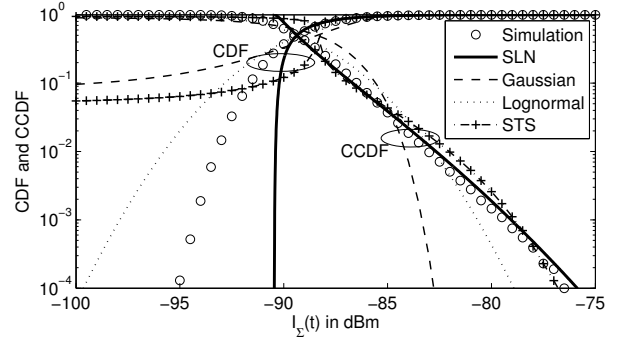
Fig. 2. Comparison of CDF and CCDF of $I_{\Sigma}(t)$ from different models.
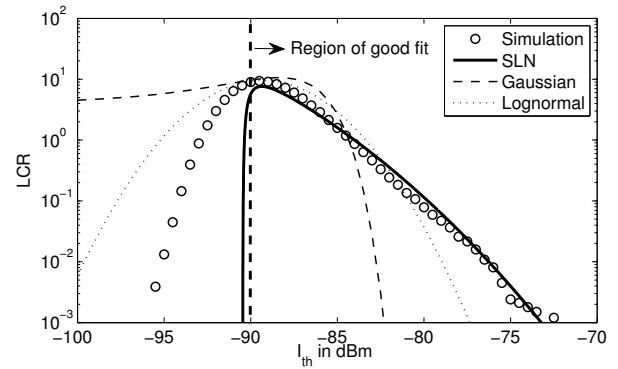
Fig. 3. Comparison of LCR of $I_{\Sigma}(t)$ from different models.

matches the LCR accurately, and is the most accurate model. As mentioned, corresponding results for the STS model are not shown because a time-varying model for it is not known.

We now study in Fig. 4 the AED of $I_{\Sigma}(t)$ using the various models. We observe that the AED curve monotonically decreases as $I_{\Sigma}(t)$ increases from zero to ∞. As before, the Gaussian RP model does not accurately track the AED of $I_{\Sigma}(t)$ for smaller and larger values of I_{th}. As before, the SLN model provides the best match for the AED for $I_{\text{th}} > -90$ dBm. The above results hold true for larger and smaller values of Υ, and for σ_{x_i} and σ_{y_i} up to 10.

A. Application to PEZ Design

We now use the interference model developed above to redesign the PEZ based on two constraints. The first constraint is the outage constraint, which mandates that the probability that the aggregate interference $I_{\Sigma}(t)$ is greater than I_{th} should not exceed $1 - \rho$ [11]. The second constraint, which is new, is the AED constraint. It mandates that the average time duration for which $I_{\Sigma}(t)$ remains above I_{th} should not exceed δ. The problem can be formulated as:

$$\min \quad R_{\text{PEZ}}$$
$$\text{subject to} \quad \Pr(I_{\Sigma}(t) \geqslant I_{\text{th}}) \leqslant 1 - \rho, \quad (15)$$
$$\text{AED}_{I_{\Sigma(t)}}(I_{\text{th}}) \leqslant \delta. \quad (16)$$
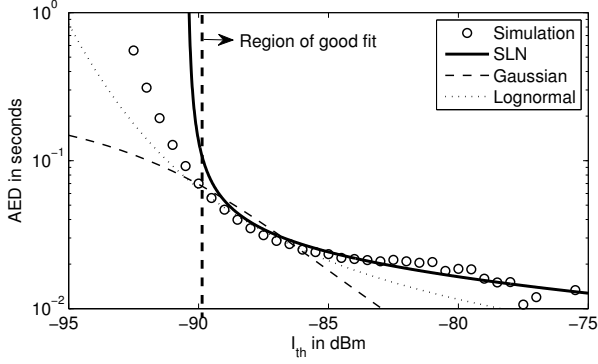
Fig. 4. Comparison of AED of $I_\Sigma(t)$ from different models.
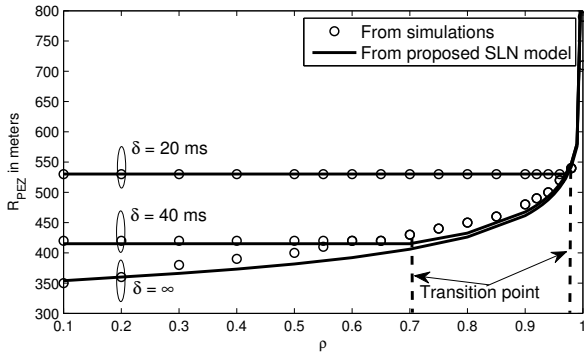
Fig. 5. PEZ radius as a function of ρ using the SLN process model.

The optimal value of R_{PEZ} that satisfies the constraints is determined analytically from the proposed SLN RP model and compared with Monte Carlo simulations, which use 5000 drops. Figure 5 plots R_{PEZ} as a function of ρ for different δ for $I_{\text{th}} = -95$ dBm. Only the outage constraint is active when $\delta = \infty$. As ρ increases, the outage constraint becomes tighter and R_{PEZ} increases. For $\delta = 40$ ms, the AED is the active constraint for $\rho < 0.70$. When δ is reduced to 20 ms, the AED constraint is the active constraint for ρ as large as 0.97.

V. CONCLUSIONS

We saw that the shifted lognormal random process model accurately characterizes the aggregate interference for interference values that exceed its shift. Our model takes into account several sources of randomness such as imperfect SS, time-correlated shadowing and fading, and randomness in the number of SUs and their locations. It is considerably more accurate than the Gaussian and lognormal RP models. It is more accurate than the STS model, which only models the PDF but not the time-variations. We saw that all the considered models, including the proposed model, failed to accurately model the low interference regime. Accurate modeling for this remains an open problem. We also saw that the AED constraint, which the proposed model analytically characterizes, increased the radius of the PEZ except when the interference

outage probability constraint was very tight. The proposed model can be extended to also account for cooperative SS [22].

APPENDIX

A. Derivation of Covariance Functions $C_Z(\tau)$ and $C_{I_\Sigma}(\tau)$

To obtain $C_Z(\tau)$, we match the covariance functions of $I_\Sigma(t)$ and $e^{Z(t)} + s$. It can be shown that the covariance function of the latter is given by

$$C_{e^{Z(t)}+s}(\tau) = e^{2\mu_Z + \sigma_Z^2 + C_Z(\tau)} - e^{2\mu_Z + \sigma_Z^2}. \quad (17)$$

The covariance function $C_{I_\Sigma}(\tau)$ of $I_\Sigma(t)$ is given by

$$C_{I_\Sigma}(\tau) = \mathbb{E}\left[\sum_{i=1}^{N_{CR}} I_i(t) \sum_{i=1}^{N_{CR}} I_j(t+\tau)\right] - \left(\mathbb{E}\left[\sum_{i=1}^{N_{CR}} I_i(t)\right]\right)^2. \quad (18)$$

Since N_{CR} and $I_i(t)$ are independent, we get

$$C_{I_\Sigma}(\tau) = \mathbb{E}[N_{CR}]\mathbb{E}[I_i(t)I_i(t+\tau)] + \mathbb{E}[N_{CR}(N_{CR}-1)]$$
$$\times \mathbb{E}[I_i(t)]\mathbb{E}[I_j(t+\tau)] - (\mathbb{E}[N_{CR}]\mathbb{E}[I_i(t+\tau)])^2. \quad (19)$$

Using $\mathbb{E}[N_{CR}] = \Upsilon A$ and $\mathbb{E}[N_{CR}^2] = \Upsilon A + (\Upsilon A)^2$, we get

$$C_{I_\Sigma}(\tau) = \Upsilon A \mathbb{E}[I_i(t)I_i(t+\tau)]. \quad (20)$$

Upon equating (17) and (20), we get (10).

B. Derivation of mth Moment of $I_i(t)$

Recall that the ith SU transmits with power P_o if it detects the PU-Tx to be off, which happens with probability $P_D(q_i, Y_i, g_i)$. Else, it transmits with power P_u. From the law of total probability and (5), we can write

$$\mathbb{E}[I_i(t)^m] =$$
$$\mathbb{E}\left[\left(P_o K \left(\frac{d_0}{r_i(t)}\right)^\eta e^{\beta X_i(t)} h_i(t)\right)^m (1 - P_D(q_i, Y_i, g_i))\right]$$
$$+ \mathbb{E}\left[\left(P_u K \left(\frac{d_0}{r_i(t)}\right)^\eta e^{\beta X_i(t)} h_i(t)\right)^m P_D(q_i, Y_i, g_i)\right]. \quad (21)$$

Since $X_i(t)$ is independent of the RVs $r_i(t)$, q_i, Y_i, and g_i, rearranging terms results in

$$\mathbb{E}[I_i(t)^m] = P_o^m K^m \mathbb{E}\left[\left(\frac{d_0}{r_i(t)}\right)^{m\eta}\right] \mathbb{E}\left[e^{m\beta X_i(t)}\right] \mathbb{E}[h_i(t)^m]$$
$$- (P_o^m - P_u^m) K^m \mathbb{E}\left[e^{m\beta X_i(t)}\right] \mathbb{E}[h_i(t)^m]$$
$$\times \mathbb{E}\left[\left(\frac{d_0}{r_i(t)}\right)^{m\eta} P_D(q_i, Y_i, g_i)\right]. \quad (22)$$

Using $\mathbb{E}[h_i(t)^m] = m!$, the moment generating function (MGF) of $X_i(t)$, and the PDFs of Y_i and g_i, we get

$$\mathbb{E}[I_i(t)^m] = m! P_o^m K^m e^{\frac{1}{2}m^2\beta^2\sigma_{x_i}^2} \mathbb{E}\left[\left(\frac{d_0}{r_i(t)}\right)^{m\eta}\right]$$
$$- m!(P_o^m - P_u^m) K^m e^{\frac{1}{2}m^2\beta^2\sigma_{x_i}^2} \frac{1}{\sigma_{y_i}\sqrt{2\pi}} \int_{-\infty}^{\infty} e^{-\frac{y_i^2}{2\sigma_{x_i}^2}}$$
$$\times \int_0^{\infty} e^{-g_i} \mathbb{E}\left[\left(\frac{d_0}{r_i(t)}\right)^{m\eta} P_D(q_i, y_i, g_i)\right] dg_i \, dy_i. \quad (23)$$

Using Gauss-Hermite and Gauss-Laguerre quadratures [17] to evaluate the integrals over y_i and g_i, respectively, yields

$$\mathbb{E}[I_i(t)^m] \approx m! P_o^m K^m e^{\frac{1}{2}m^2\beta^2\sigma_{x_i}^2} \mathbb{E}\left[\left(\frac{d_0}{r_i(t)}\right)^{m\eta}\right]$$

$$-\frac{m!}{\sqrt{\pi}}\left(P_o^m - P_u^m\right) K^m e^{\frac{1}{2}m^2\beta^2\sigma_{x_i}^2} \sum_{n_1=1}^{W_h} w_h(n_1) \sum_{n_2=1}^{W_l} w_l(n_2)$$

$$\times \mathbb{E}\left[\left(\frac{d_0}{r_i(t)}\right)^{m\eta} P_D\left(q_i, \sqrt{2}\sigma_{y_i} a_h(n_1), a_l(n_2)\right)\right], \quad (24)$$

where $q_i = \sqrt{r_i(t)^2 + p^2 - 2r_i(t)p\cos\theta}$ and θ is uniformly distributed over $[0, 2\pi]$.

Substituting the PDF of θ and using Gauss-Chebyshev quadrature [17] to evaluate the integral over θ yields

$$\mathbb{E}[I_i(t)^m] \approx m! P_o^m K^m e^{\frac{1}{2}m^2\beta^2\sigma_{x_i}^2} \mathbb{E}\left[\left(\frac{d_0}{r_i(t)}\right)^{m\eta}\right]$$

$$-\frac{m!}{\sqrt{\pi}W_c}\left(P_o^m - P_u^m\right) K^m e^{\frac{1}{2}m^2\beta^2\sigma_{x_i}^2} \sum_{n_1=1}^{W_h} w_h(n_1) \sum_{n_2}^{W_l} w_l(n_2)$$

$$\times \sum_{n_3=1}^{W_c} \mathbb{E}\left[\left(\frac{d_0}{r_i(t)}\right)^{m\eta} P_D\left(q_i'(r_i(t), n_3), \sqrt{2}\sigma_{y_i} a_h(n_1), a_l(n_2)\right)\right],$$

where $q_i'(r_i(t), n_3) = \sqrt{r_i(t)^2 + p^2 - 2r_i(t)pa_c(n_3)}$. Given the total number of SUs, the location of the ith SU is uniformly distributed over the region for an SPPP. Writing in terms of the PDF of $r_i(t)$ and simplifying yields (11).

C. Brief Derivation of Autocorrelation of $I_i(t)$

Along lines similar to Appendix B, the autocorrelation of $I_i(t)$ can be written as

$$\mathbb{E}[I_i(t)I_i(t+\tau)] = P_o^2 K^2 \mathbb{E}\left[e^{\beta(X_i(t)+X_i(t+\tau))}\right]$$

$$\times \mathbb{E}[h_i(t)h_i(t+\tau)]\mathbb{E}\left[\left(\frac{d_0^2}{r_i(t)r_i(t+\tau)}\right)^{\eta}\right]$$

$$-\left(P_o^2 - P_u^2\right)K^2\mathbb{E}\left[e^{\beta(X_i(t)+X_i(t+\tau))}\right]\mathbb{E}[h_i(t)h_i(t+\tau)]$$

$$\times \mathbb{E}\left[\left(\frac{d_0^2}{r_i(t)r_i(t+\tau)}\right)^{\eta} P_D(q_i, Y_i, g_i)\right]. \quad (25)$$

Since the distance $r_i(t)$ between the ith SU and the PU-Rx is typically larger than the distance traveled by the SU in a time duration τ, $r_i(t+\tau) \approx r_i(t)$. Rearranging terms and substituting the joint MGF of $X_i(t)$ and $X_i(t+\tau)$ (by using (2)) and the autocorrelation of $h_i(t)$ and $h_i(t+\tau)$, we get

$$\mathbb{E}[I_i(t)I_i(t+\tau)] \approx P_o^2 K^2 e^{\beta^2\sigma_{x_i}^2\left(1+\exp\left(\frac{-v^2\tau^2}{2D^2}\right)\right)} \mathbb{E}\left[\frac{d_0^{2\eta}}{r_i(t)^{2\eta}}\right]$$

$$\times \left(J_0^2(2\pi f_m\tau) + 1\right) - \left(P_o^2 - P_u^2\right)K^2 e^{\beta^2\sigma_{x_i}^2\left(1+\exp\left(-\frac{v^2\tau^2}{2D^2}\right)\right)}$$

$$\times \left(J_0^2(2\pi f_m\tau) + 1\right)\mathbb{E}\left[\left(\frac{d_0}{r_i(t)}\right)^{2\eta} P_D(q_i, Y_i, g_i)\right]. \quad (26)$$

Averaging over the RVs Y_i, g_i, and θ, as in Appendix B, substituting the PDF of $r_i(t)$, and simplifying yields (12).

REFERENCES

[1] M. Hanif, M. Shafi, P. Smith, and P. Dmochowski, "Interference and deployment issues for cognitive radio systems in shadowing environments," in *Proc. ICC*, pp. 1–6, Jun. 2009.

[2] Z. Chen, C.-X. Wang, X. Hong, J. S. Thompson, S. A. Vorobyov, X. Ge, H. Xiao, and F. Zhao, "Aggregate interference modeling in cognitive radio networks with power and contention control," *IEEE Trans. Commun*, vol. 60, pp. 456–468, Feb. 2012.

[3] A. Rabbachin, T. Q. S. Quek, H. Shin, and M. Z. Win, "Cognitive network interference," *IEEE J. Sel. Areas Commun.*, vol. 29, pp. 480–493, Feb. 2011.

[4] A. Ghasemi and E. S. Sousa, "Interference aggregation in spectrum-sensing cognitive wireless networks," *IEEE J. Sel. Topics Signal Process.*, vol. 2, pp. 41–56, Feb. 2008.

[5] G. Stuber, S. Almalfouh, and D. Sale, "Interference analysis of TV-band whitespace," *Proc. IEEE*, vol. 97, pp. 741–754, Apr. 2009.

[6] P. Talmola, J. Kalliovaara, J. Paavola, R. Ekman, A. Vainisto, N. Aurala, H. Kokkinen, K. Heiska, R. Wichman, and J. Poikonen, "Field measurements of WSD-DTT protection ratios over outdoor and indoor reference geometries," in *Proc. CROWNCOM*, pp. 7–12, Jun. 2012.

[7] A. Ben Hadj Alaya-Feki, B. Sayrac, S. Ben Jemaa, and E. Moulines, "Interference cartography for hierarchical dynamic spectrum access," in *Proc. DySPAN*, pp. 1–5, Oct. 2008.

[8] A. Goldsmith, S. A. Jafar, I. Maric, and S. Srinivasa, "Breaking spectrum gridlock with cognitive radios: An information theoretic perspective," *Proceedings of the IEEE*, vol. 97, pp. 894–914, Apr. 2009.

[9] M. Win, P. Pinto, and L. Shepp, "A mathematical theory of network interference and its applications," *Proc. IEEE*, vol. 97, pp. 205–230, Feb. 2009.

[10] J. Lai and N. Mandayam, "Minimum duration outages in Rayleigh fading channels," *IEEE Trans. Commun*, vol. 49, pp. 1755–1761, Oct. 2001.

[11] M. Vu, N. Devroye, and V. Tarokh, "On the primary exclusive region of cognitive networks," *IEEE Trans. Wireless Commun.*, vol. 8, pp. 3380–3385, Jul. 2009.

[12] A. Bagayoko, P. Tortelier, and I. Fijalkow, "Impact of shadowing on the primary exclusive region in cognitive networks," in *Proc. Eur. Wireless Conf.*, pp. 105–110, Apr. 2010.

[13] P. Smith, H. Suraweera, and M. Shafi, "Signal power variation with applications to cognitive radio," in *Proc. Commun. Theory Workshop*, pp. 33–38, Feb. 2008.

[14] M. Hanif and P. Smith, "Level crossing rates of interference in cognitive radio networks," *IEEE Trans. Wireless Commun.*, vol. 9, pp. 1283–1287, Apr. 2010.

[15] G. L. Stüber, *Principles of Mobile Communications*. Kluwer Academic Publishers, 1996.

[16] A. J. Goldsmith, *Wireless Communications*. Cambridge Univ. Press, 2005.

[17] M. Abramowitz and I. Stegun, *Handbook of Mathematical Functions with Formulas, Graphs, and Mathematical Tables*. Dover, 9 ed., 1972.

[18] A. Sonnenschein and P. M. Fishman, "Radiometric detection of spread-spectrum signals in noise of uncertain power," *IEEE Trans. Aerosp. Electron. Syst.*, vol. 28, pp. 654–660, Jul. 1992.

[19] T. Yucek and H. Arslan, "A survey of spectrum sensing algorithms for cognitive radio applications," *IEEE Commun. Surv. Tutorials*, vol. 11, pp. 116–130, Mar. 2009.

[20] J. J. Lehtomaki, "Performance comparison of multichannel energy detector output processing methods," in *Proc. Int. Symp. Signal Process. App.*, pp. 261–264, Jul. 2003.

[21] C. Fischione, F. Graziosi, and F. Santucci, "Approximation for a sum of on-off lognormal processes with wireless applications," *IEEE Trans. Commun*, vol. 55, pp. 1984–1993, Oct. 2007.

[22] M. Shabbir Ali and N. B. Mehta, "Modeling time-varying aggregate interference in cognitive radio systems, and implications on primary exclusive zone design," *Submitted*, 2013.